T. Kim

C W. Wang

Department of Mechanical Engineering,
University of Michigan,
2250 G.G. Brown Building,
2350 Hayward Street,
Ann Arbor, MI 48109-2125

F. I. M. Thomas
University of Hawaii,
Hawaii Institute of Marine Biology,
P. O. Box 1346,
Kaneohe, HI 96744

A. M. Sastry[1]
Fellow ASME
Departments of Mechanical, Biomedical
and Materials Science and Engineering,
University of Michigan,
Ann Arbor, MI 48109-2125
e-mail: amsastry@umich.edu

Fluid-Structure Interaction Analysis of Flow-Induced Deformation in a Two-Phase, Neo-Hookean Marine Egg

Coupled computational fluid dynamics and finite element analyses were used to determine the material properties of the egg and jelly layer of the sea urchin Arbacia punctulata. Prior experimental shear flow results were used to provide material parameters for these simulations. A Neo-Hookean model was used to model the hyperelastic behaviors of the jelly layer and egg. A simple compressive simulation was then performed, to compare the maximum von Mises stresses within eggs, with and without jelly layers. Results of this study showed that (1) shear moduli range from ~100 to 160 Pa*, and* ~40 to 140 Pa *for an egg without a jelly layer, and jelly layer itself, respectively; and (2) the presence of the jelly layer significantly reduces maximum von Mises stress in an egg undergoing compression.* [DOI: 10.1115/1.2345443]

1 Introduction

The extracellular matrix surrounding the sea urchin egg has been intensively studied because of its importance in fertilization [1–6]. Possible roles of this so-called "jelly layer" include chemoattraction of sperm, via the speract [7,8], and resact [7–12] peptides; prevention of polyspermy [13–15]; increasing collision frequency with sperm because of its effect of increasing the overall size of the egg [14,16–19]; and promotion of species-specific interaction between sperms and eggs [20–22]. Protection of the egg from mechanical forces [23–26] appears to be another possible role of the jelly layer, given the relatively large stresses to which the egg is exposed [26], and the clearly negative effect that high stress has on fertilizability of the egg [26,27].

The jelly layer of *Arbacia punctulata* [14,26,27] is the subject of the present study. Figure 1 shows an optical microscope image of the egg with a jelly layer, submerged in a solution of seawater mixed with Sumi ink. The latter cannot penetrate the jelly coat, and thus allows visualization of the layer as a translucent ring around the egg.

Two distinct phases of application of shear stresses to eggs occur naturally. First, during spawning, shear stresses of up to 58.7 Pa can be transferred to the egg, since the diameter of the rigid, calcified gonopore through which the egg passes is frequently smaller than the egg diameter [26,28]. Second, after spawning, the jelly-coated eggs are exposed to stresses in the water column, of ~1.9–4 Pa [29]. In this second phase, jelly coats also undergo hydration, increasing their diameters from ~78 to ~127 μm. After a short period of hydration, jelly coats dissolve in the seawater [26].

1.1 Prior Art and Previous Findings: Stresses Experienced by A. Punctulata eggs. Prior approaches to measure material properties of single cells have involved use of atomic force microscopy [30,31]; magnetic twisted bead microrheometry [32]; micropipette aspiration [33]; microplate compression [34]; use of optical tweezers [35]; and shear flow experiments [36–38]. The first two approaches utilize probes or beads to induce local deformation, and thus allow estimation of material properties. The remaining approaches employ whole-cell deformation to determine material properties.

In assaying the particular mechanical properties of sea urchin eggs, parallel plate compression [39] and glass rod [39] have been used. Similarly, compression tests have been conducted to measure the mechanical properties of the blastula wall of the sea urchin eggs in a channel filled with seawater [40].

There is ample experimental evidence by both our own group [41], and others [26,27] of the clear and quantifiable differences in the mechanical properties of the jelly layer and the egg. Recently, we used a shear flow experiment to investigate the mechanical properties of *Arbacia punctulata* eggs [41]. The setup for the shear flow experiment comprised a peristaltic pump, flow channel (Fig. 2), inverted microscope (Ts100, Nikon), digital camera (C4742-95-12ERG, Hamamatsu), storage tank, and image processing software (C.IMAGE system). Jelly-coated and jelly-free sea urchin eggs were pipetted onto a silane glass slide; the slide was then inserted into the channel. The channel was constructed of Plexiglas (Warp Bros Co.), with dimensions 25 mm $\times$ 2 mm $\times$ 400 mm (W $\times$ H $\times$ L). Artificial seawater was circulated between the tank and the channel in a closed loop. The sea urchin eggs were deformed by circulated seawater solution; shear stresses were adjusted by controlling flow rate of the seawater solution, via control of the peristaltic pump speed. Applied shear stresses on the external surface of eggs were approximated based on an assumption of Poiseuille flow between two parallel plates.

Deformations of the eggs were recorded digitally for analysis, as shown in Fig. 3. A shear stress of ~21.6 Pa was shown to be capable of removal of the jelly layer from the egg, and a shear stress of ~23.9 Pa resulted in egg rupture. The flow rates required to induce shear stresses of 21.6, and 23.9 Pa were ~3.42 $\times 10^{-6}$ m^3/s and ~7.42 $\times 10^{-6}$ m^3/s, respectively, for our apparatus (Fig. 2).

[1]Corresponding author.

Contributed by the Materials Division of ASME for publication in the JOURNAL OF ENGINEERING MATERIALS AND TECHNOLOGY. Manuscript received February 6, 2006; final manuscript received June 19, 2006.

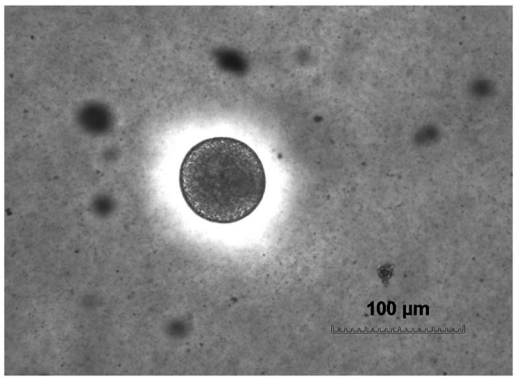

Fig. 1 Egg and jelly layer of a sea urchin *Arbacia punctulata* (×200); Sumi ink was used for visualization

1.2 Use of the Fluid-Structure-Interaction (FSI) Approach in Determining Material Properties From Experimental Response. Our prior data on deformation histories of jelly-coated Arbacia punctulata eggs [41] were used to inform an inverse analysis, as done by previous groups, for example, in extracting tissue properties [42,43] and the separate properties of membranes and cells [42,44,45]. Kauer et al. [45] and Seshaiyer and Humphrey [44] assumed viscoelastic, and neo-Hookean, Mooney-Rivlin, and Fung-exponential hyperelastic material models, respectively. Caille et al. [42] similarly used a neo-Hookean model to determine the constitutive response of the nucleus of a bovine endothelial cell.

As in those cases, the material properties of jelly layer and egg were unknown initially. Thus, in the present work, material properties and recorded flow conditions obtained from prior shear flow experiments were compared iteratively, until deformations of the model and recorded images matched.

1.3 Objectives of Present Study. We restricted our study to partially hydrated eggs. Our principal interest was in developing a robust method of determining the separate mechanical properties of the egg and the jelly coat, with the understanding that jelly coat properties are dramatically altered by hydration. In order to prevent dissolution of the jelly coat, a preservative was used in our microfluidic experiments, described elsewhere [41] and outlined here as well. Our specific objectives were twofold:

(1) To determine the properties of the partially hydrated jelly layer and egg through matching of simulation/experimental data; and
(2) to determine conditions under which the presence of a partially hydrated jelly layer reduces stress experienced by the gamete.

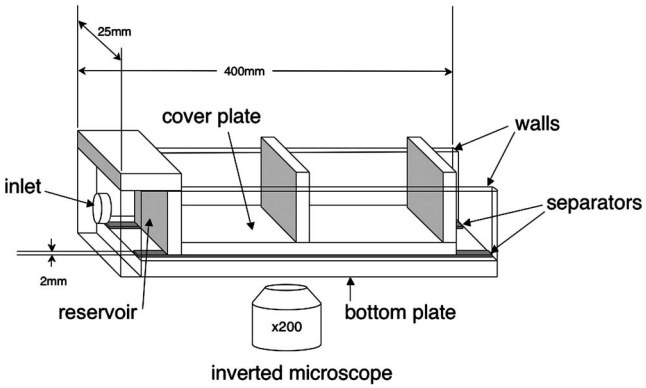

Fig. 2 Detailed schematic of the flow channel; adapted from [41]

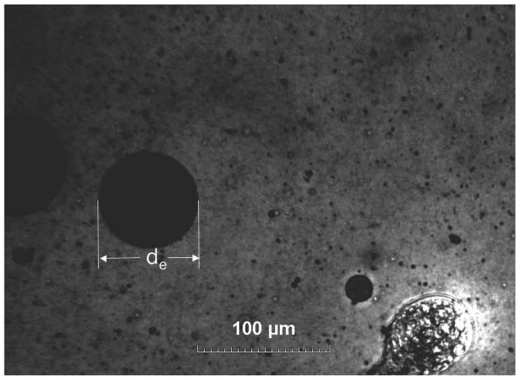

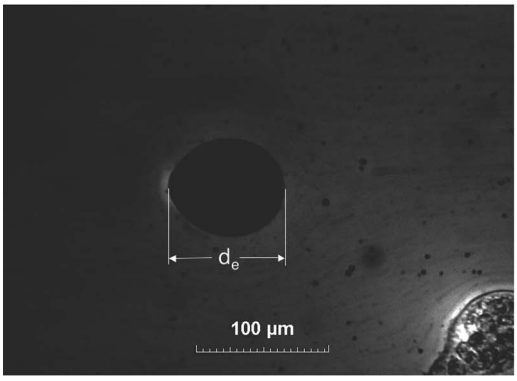

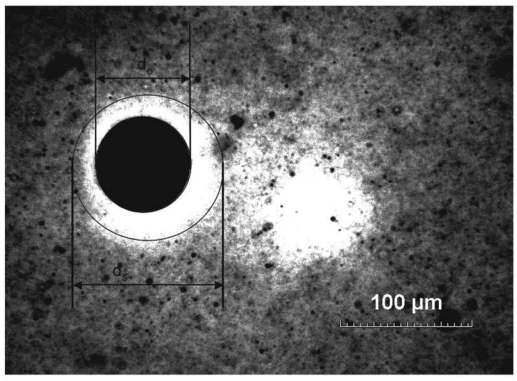

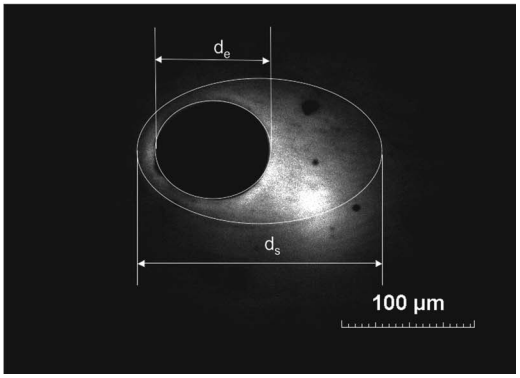

Fig. 3 Sample images obtained from the shear flow experiments of [41], showing definitions of (*a*) diameter, d_e, of egg without jelly layer and without application of shear stress, (*b*) diameter of major axis length, d_e, of egg without jelly layer under a shear flow rate of 3.42×10^{-6} m^3/s, (*c*) diameters of egg, d_e, and outer surface of jelly layer, d_s, without application of shear stress, and (*d*) diameters of major axis length of egg, d_e, and outer surface of jelly layer, d_s, under a shear flow rate of $3.42\ 10^{-6}$ m^3/s

Table 1 Experimental parameters[41] used as input for FSI simulations

		Experimental results		Fluid conditions (input)	
	Egg Number	Undeformed $d_e/\mathbf{d_s}$ (μm)	Deformed d_s (μm)	Velocity at 300 μm (μm/s)	Viscosity (Pa s)
Group 1	1–4 Egg alone	76.44±3.12	88.83±3.57	66,150	0.104
Group 2	5,6	80.55±1.49/ **102.63±2.19**	120±0	95,400	0.076
Group 3	7	72.1/**107.4**	161.1	61,560	0.111
Group 4	8	71.6/**95.8**	139.0	61,560	0.111

We restricted our numerical considerations to these two questions, and emphasize that validation of the selective role of the jelly coat in mechanical protection does not invalidate, in and of itself, other roles, including sperm chemotaxis. However, future work will focus exactly on the question of the relative importance of all of these roles.

2 Methods

2.1 General Numerical Approach. Our numerical analyses comprised coupled computational fluid dynamics (CFD) and structural analyses. The inverse-coupled finite element method (FEM) was implemented in a commercial FEM package, ANSYS© (Version 7.0, March 2004, ANSYS Inc.). Three-dimensional models were created by the preprocessing toolbox in ANSYS©. Diameters of eggs with jelly coat, d_e and eggs only, d_s, under deformed and unreformed conditions, and parameters describing the shear flow experiment in [41] are listed in Table 1. Egg and jelly layer materials were assumed to be homogeneous, isotropic, and hyperelastic in the structural analysis, based on prior findings [41]. A laminar flow assumption was used in the CFD analysis. Mathematical models were built separately for each (CFD and FE) analysis. Updated information, including geometry of the egg, jelly layer, and flow conditions, was exchanged between these two analyses through the nodes at the egg surfaces. Hexahedral elements were used for the inlet and outlet zones, and tetrahedral elements were used for the buffer zone; a transient, pyramidal element was used to bridge the hexahedral and tetrahedral elements in the buffer zone as in Fig. 4.

2.2 CFD Analysis: Governing Equations and Implementation. The CFD analysis was separated into three zones: inlet and outlet zones, a transient zone, and a buffer zone, as shown in Fig. 4. The inlet and outlet zones were continuous, since we applied periodic boundary conditions; each of these zones was meshed with hexahedral elements. The buffer zone was meshed with tetrahedral elements to improve remeshability during analysis. The total number of elements for CFD was about 5000. No-slip conditions were set for all planes comprising the flow channel, except the two transverse planes of inlet and outlet, the longitudinal plane through the center of the egg, and the egg surface. Symmetric boundary conditions were set at the plane through the center of the egg, along the flow direction of the CFD analysis, to reduce computational effort. All boundary conditions for the CFD analysis are shown in Table 2.

Prior experimental results [41] were used to calculate a Reynold's number, R_e, around the eggs, of $\sim 5.5\times10^{-3}$–2.4×10^{-2}, which was less than the critical value of 5 [46]. Thus, Newtonian, laminar flow was assumed for a region sufficiently far from the egg. The continuity and momentum equations are written, respectively, as

$$\nabla \cdot \mathbf{u} = 0, \quad \text{and} \tag{1}$$

$$\nabla p = \mu \nabla^2 \mathbf{u} \tag{2}$$

where $\mathbf{u}$ is the velocity vector of fluid, p is pressure, and μ is the dynamic viscosity of the fluid. For our simple channel geometry, with a no-slip boundary condition on the walls of the plates, analytic solutions of Eqs. (1) and (2) yield the well-known velocity profile u, as

$$u = \frac{6Q}{WH^3}(Hy - y^2) \tag{3}$$

shear rate, S, as

$$S = \frac{d\theta}{dt} = \frac{du}{dy} = \frac{6Q}{WH^3}(H - 2y) \tag{4}$$

and shear stress, τ, as

$$\tau = \mu\frac{6Q}{WH^3}(H - 2y) \tag{5}$$

In all of these relations, Q is the flow rate, y is the distance from the surface of the bottom plate, μ is the dynamic viscosity, and W and H are the channel width and height, respectively.

The depth of the channel used in our shear flow experiment was

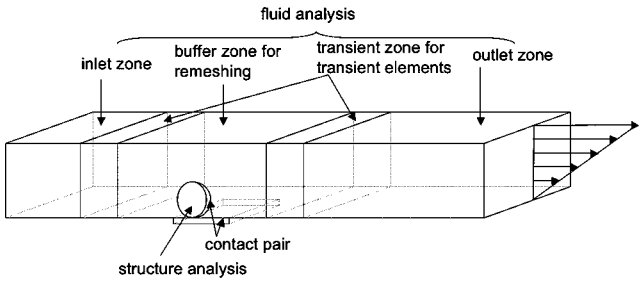

Fig. 4 Schematic of the CFD analysis; region 1 is divided into inlet and outlet, transient, and buffer zones. Region 2 was used for structural analysis.

Table 2 Boundary conditions for FSI simulations

		Fluid analysis	Structural analysis
Regions (element)	Region 1	Fluid	Null
	Region 2	Null	Egg
Boundary conditions	Top	Moving plate	⋯
	Bottom	Fixed (velocities)	⋯
	Front	Symmetric	Symmetric
	Back	Symmetric	⋯
	$\text{Side}_{\text{inlet}}$	Periodic	⋯
	$\text{Side}_{\text{outlet}}$	Periodic	⋯
	Egg surface	No slip	Loading from fluid
	Egg bottom	⋯	fixed (displacements)

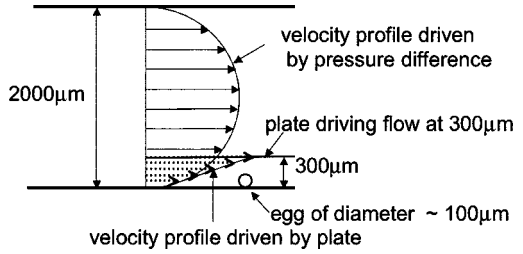

Fig. 5 Schematic comparing relative sizes of eggs and channel, and velocity profile between two parallel plates. Approximate velocity profile of the simulated region was obtained by linearization of the parabolic velocity profile, near the bottom (<300 μm).

~2 mm, which is much larger than the size of an egg with a jelly layer (~100 μm). The simple flow described above becomes complicated near the egg, at the bottom of the channel. Hence, only the region around the egg was analyzed numerically; dimensions of the modeled region were approximately 300 μm $\times$200 μm$\times$1600 μm (H$\times$W$\times$L). Due to the relatively small height of the modeled region, the input flow velocity was simplified by linearization of Eq. (3), as

$$u_{\text{linearized}} = \frac{6Q}{WH^2}y \tag{6}$$

as shown in Fig. 5. Thus, the input flow velocity profile for the height of 300 μm of localized CFD model was reduced to

$$u_{300} = 18{,}000 \cdot Q\text{m/s} \tag{7}$$

No-slip boundary conditions were set on both the surfaces of glass slide and egg in this study.

Shear stresses induced by the gradient of fluid velocity were treated as external loads in the structural analysis. The egg was then deformed, providing a new geometry for the next step in the fluid analysis. Criteria used for fluid, structural, and overall convergence were simply the default values in ANSYS, except for the displacement change ratio, which was set to 0.01.

2.3 Structural Finite Element Analysis: Governing Equations and Implementation. The FEM model for the structural analysis included only jelly-coated or jelly-free eggs, attached to glass slides. Satisfactory experimental determination of contact area is challenging in performing this analysis. To model exact shape changes induced by the polarization of the egg surface on the slide would be difficult at best, and at worst, impossible to model with any degree of suitable resolution in our FE models.

Thus, to investigate the effect of contact area on the material behavior in a systematic way, a degree of contact n was defined as the ratio of the distance from the slide to the top of the egg (the height of the attached egg) to the original diameter, as shown in Fig. 6. To generate a model for structural analysis, the egg was shifted downward, using the factor $(1-n)$, as shown in Fig. 6. We

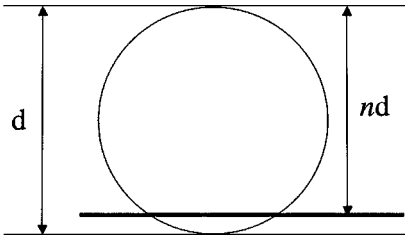

Fig. 6 Definition of degree of contact, *n*, for description of contact area

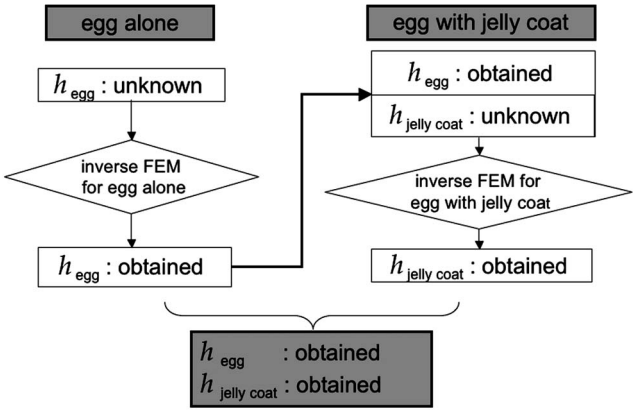

Fig. 7 Schematic representation of the strategy used to extract the shear moduli of neo-Hookean models for eggs and jelly layers

note that our use of a degree of contact is an arbitrary but convenient way of altering contact area in a systematic way, without altering the egg volume significantly.

Both the egg and jelly layer exhibited large deformations in our shear flow experiments; both phases also returned to approximately their original shapes after removal of external loads [41]. Thus, hyperelastic material models were used for each phase for structural analysis. The simplest of these, the Neo-Hookean model, requires only a shear modulus to describe material response, and was used here. Its strain energy function is

$$W = \frac{\mu(I_1 - 3)}{2} + \frac{(J-1)^2}{d} \tag{8}$$

where I_1 is the first deviatoric strain invariant, J is the determinant of the elastic deformation gradient, and d is the incompressibility parameter, defined as

$$d = \frac{2(1-2\nu)}{\mu}$$

with Poisson ratio ν and shear modulus, μ. The hyperelastic material is nearly incompressible (i.e., ν~0.5), leaving the shear modulus, μ, in Eq. (8) as the only unknown. This value is determined from

$$\mu = \frac{\partial W}{\partial I_1} \tag{9}$$

To extract material properties for each phase, we adopted the strategy shown in Fig. 7. First, the shear modulus of the Neo-Hookean model for an egg without a jelly layer was determined using the coupled-inverse finite element method described previously. Next, the calculated shear modulus of the Neo-Hookean model for the egg was inserted into the model of the coated egg. Again, the coupled-inverse finite element method was employed to obtain the shear modulus of the Neo-Hookean shear modulus of the jelly layer.

For the structural finite element analysis, an egg and the plate to which the egg was attached were modeled as a contact pair, as shown in Fig. 4, to model the condition of large deformation. The egg and jelly layer were each meshed with hexahedral elements (SOLID185). Element types CONTA174 and TARGE170 were used for contact analysis. The total number of elements was 7300 for this structural finite element analysis, which included 4900 elements for the jelly region, and 2400 for the egg.

Boundary conditions are listed in Table 2, and are described briefly as follows. For the structural analysis, the jelly layer and the egg were assumed to be perfectly bonded; thus, displacements at the interface were continuous. Only eggs which remained at-

tached to the glass slide were analyzed experimentally; hence, eggs were assumed to be perfectly bonded at the interface of the glass slide and egg. Symmetric boundary conditions were set at the plane through the egg center, along the flow direction for the structural analysis, to reduce computational effort.

In our prior work [41], eight eggs were studied experimentally. The recorded deformation histories of those eight eggs were used as a base line to extract shear moduli for the egg and jelly layer. These eight eggs had the following characteristics, which can be divided into four groups:

Group 1. In this group, properties of the eggs without jelly layers (eggs 1-4, per [41]) were averaged to determine the shear modulus of the egg.

Group 2. In this group, jelly-coated eggs (eggs 5 and 6, per [41]) were deformed under the same flow conditions, in which maximum inlet flow velocity was 0.095 m/s and the local viscosity (<300 mm from the bottom of the plate) was 0.076 Pa s.

Group 3. This group had a higher inlet velocity and viscosity than Group 2. Here, an egg with a relatively thick jelly coat (egg 7, per [41]) was modeled. The maximum inlet flow velocity was 0.061 m/s, and a local viscosity of 0.11 Pa s (<300 mm from the bottom of the plate) was used.

Group 4. The egg modeled (egg 8, per [41]) was of intermediate thickness, and the lower inlet velocity of Group 3 was used.

2.4 Implementation of Egg Deformation Simulations. Another two sets of 2D FSI models were used to determine how effectively the jelly layer mitigated load transferred to the egg. Models were generated to simulate egg passage through the smaller oviduct-gonopore complex, and stresses induced by an egg spawned into the water column. These simulations comprised fixed eggs with moving flows; to achieve this, each egg was fixed at the flow front, and the fluid speed was determined as a relative velocity to the egg. To reduce computational effort by half, an axisymmetric domain was used, as shown in Fig. 8(*a*). The first model was the average size of the eggs, measured, of 76 μm. Two concentric circles with size of 76 and 120 μm were created for the second model, representing the egg and coated egg, respectively.

Both models were meshed with quadrilateral elements FLUID141 and PLANE182 for CFD and structural analyses, respectively. Boundary conditions for CFD analysis are summarized in Fig. 8(*b*). The fluid was assumed to have a local viscosity of 0.1 Pa s.

Boundary conditions for the structure analysis are shown in Fig. 8(*c*). Shear moduli for the egg and jelly layer were set to 130 and 50 Pa. The FSI modeling experiment was done for one loop; the CFD analysis was performed first, followed by the structural analysis.

3 Results

3.1 FSI Simulations. The nonlinear increase in calculated shear modulus, μ, with increasing degree of contact is shown in Fig. 9, along the major axial length. Experimental deformations ranged from ~85 to 92 μm. The contact condition was varied from 0.93 to 0.97, resulting in a range of shear moduli from 100–160 Pa.

For group 2, an analogous dependence is shown in Fig. 10 between shear modulus and degree of contact. The curves shown were generated by assuming a shear modulus of 130 Pa for the egg; calculated shear moduli for the jelly layer ranged from 118 to 148 Pa, using experimental values [41], and a range of degree of contact, n, from 0.92 to 0.94.

For group 3, shear moduli for jelly layers ranged from 55 to 65 Pa (Fig. 11); these results were based on comparison between the deformed axial length d_s obtained from the FEM models and from d_s=161 μm, obtained from experimental results [41]. The degree of contact, n, ranged from 0.95 to 0.97. In this group, a shear modulus of 130 Pa was used for the egg, as in group 2.

In group 4, the shear modulus for jelly layer ranged from 48 to 64 Pa (Fig. 12); these results were based on comparison

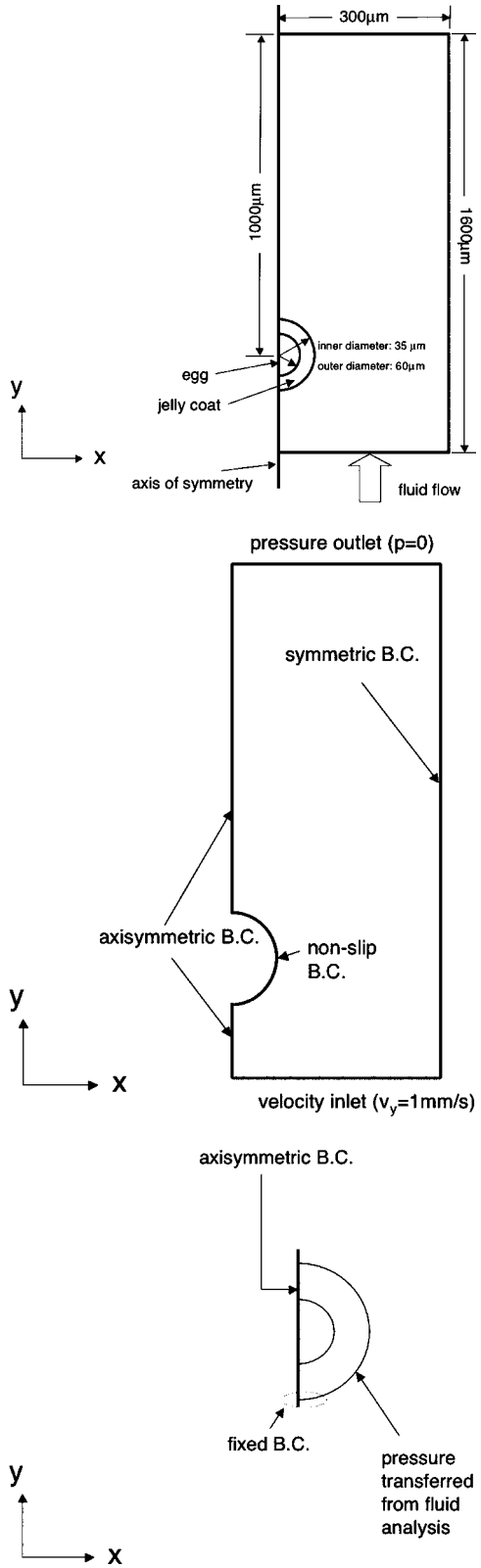

Fig. 8 Schematic representations of the FSI model to simulate the egg, with or without a jelly layer, under shear stress due to fluid flow. The dimensions of the model are shown in (*a*); boundary conditions used in CFD and structural analyses are shown in (*b*) and (*c*), respectively.

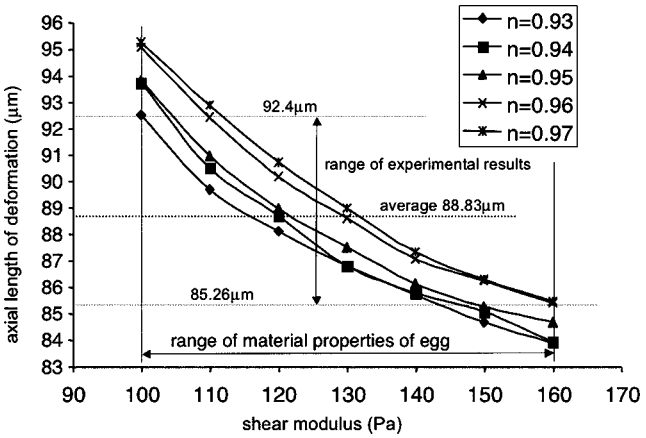

Fig. 9 Simulation results for group 1

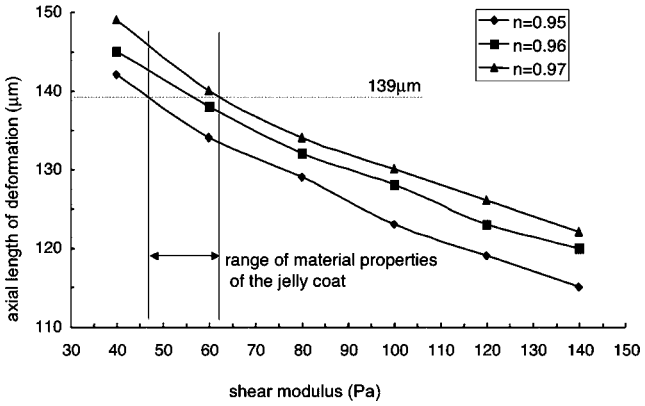

Fig. 12 Simulation results for group 4

between the deformed axial length, d_s, obtained from the FEM models and from the deformed axial length, $d_s = 139$ μm, obtained from experimental results [41]. The degree of contact, n, ranged from 0.95 to 0.97, as in group 3. In this group, a shear modulus of 130 Pa was used for the egg, as in groups 2 and 3.

3.2 Simulation Results: 2D. Our 2D FSI simulations assumed that the egg and jelly layer had shear moduli of 130 and 50 Pa, respectively; the diameter of egg and the thickness of the jelly layer were 76 and 22 μm, respectively. These parameters were chosen to simulate the egg after spawning, when the jelly layer becomes hydrated. Two simulations, for eggs with and without a jelly layer, were run for a fluid with relative velocity of 1 mm/s. The von Mises stress contours for the egg alone, and the egg with jelly layer, are shown in Figs. 13(*a*) and 13(*b*), respectively. The maximum von Mises stress in the egg without a jelly layer, for a fluid velocity of 1 mm/s and viscosity of 0.1 Pa s, was shown to be ~37.8 Pa. The maximum von Mises stress in egg with a jelly layer under the same flow conditions was determined to be ~22.9 Pa.

4 Discussion

Calculated properties in general exhibited a rather wide variation, in part due to intrinsic specimen variation, and also due to necessary assumptions in analyses. Our findings were generally

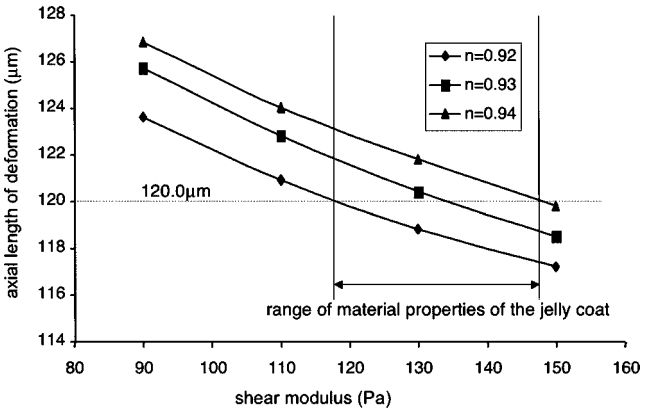

Fig. 10 Simulation results for group 2

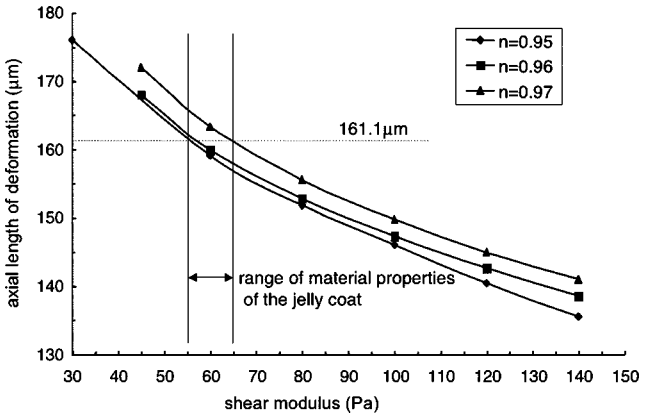

Fig. 11 Simulation results for group 3

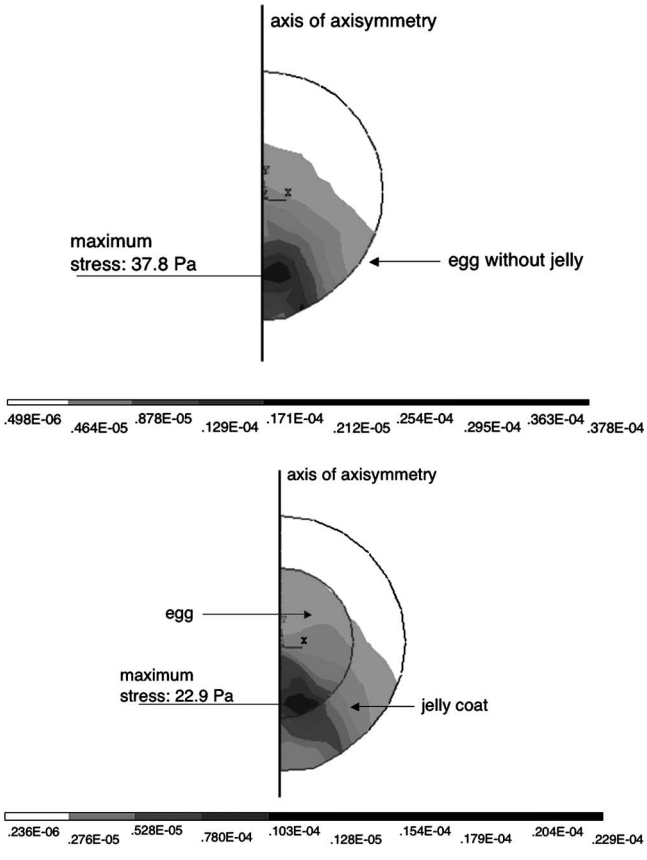

Fig. 13 Contour plots of von Mises stresses in an egg (*a*) without a jelly layer, and (*b*) with an intact jelly layer, each under an axisymmetric, compressive strain of 0.1

consistent with prior workers' results in experimental and morphological studies on the eggs, while providing a more precise range of shear moduli, and quantifying the effects of the jelly coat on mitigating load within the egg.

Calculated shear moduli exhibited a wide standard deviation, due to uncertainty in contact conditions. Shear moduli of the jelly layer for groups 2–4 ranged from 48 to 148 Pa. As shown in Figs. 10–12, the predicted shear modulus increased with increasing n, reflecting the additional resistance of the egg to rotation, with increased contact area. Shear modulus of the jelly layer for cases 3 and 4 was in a smaller relative range of 48–55 Pa, for jelly-layer thicknesses of 35 and 24 μm, respectively.

Interestingly, the highest average shear modulus for the jelly layer was found for the two eggs with the thinnest jelly layers, simulated by group 2; this was nearly double the average value for the eggs of groups 3 and 4. This finding appears consistent with the morphological findings of Bonnell et al. [5], which showed that the fiber density of the jelly layer is higher, close to the egg surface. We have extensively studied the effect of local density on such networks [43]; collectively, these results suggest that heterogeneity in the jelly layer may be an important consideration in determining its effect on fertilizability.

As shown in Fig. 13, the maximum von Mises stresses of eggs with and without jelly layer were, respectively, 37.8 and 22.9 Pa, under the same strain. Thus, the maximum von Mises stress of an egg with jelly layer was reduced by almost 39% compared to the one for an egg without jelly coat. This is clear evidence of protection for the egg by the jelly layer.

5 Conclusions and Future Work

Though our overall approach represented both detailed experimental and numerical analyses, it is challenging to separately, experimentally determine the material properties of jelly layer and egg. Our strategy, incorporating a shear flow experiment and finite element method, can be used to determine the material properties of each phase nondestructively, and further allows full visualization of the pre- and post-rupture behavior of the egg.

Our findings suggested a protective role for the jelly coat, given the reduction in stresses on the egg observed by FE simulation using neo-Hookean parameters obtained by FSI. Some issues, however, clearly bear further scrutiny. These include the health of the sea urchin, and effect of diet, weather, and season. Future work will incorporate more experimental parameters for deformation, and specifically compare the probable, nonexclusive selective roles of the jelly coat in both mechanical protection and as a sperm chemoattractant.

Acknowledgment

Support for this work was provided by DARPA and ONR through the Synthetic Multifunctional Materials (SMFM) Program (Dr. Leo Christodoulou and Dr. Steve Fishman, Program Monitors), from a NSF PECASE (Sastry), and the W.M. Keck Foundation is gratefully acknowledged.

References

[1] Kitazume, S., Kitajima, K., Inoue, S., Troy, F. A., Cho, J. W., Lennarz, W. J., and Inoue, Y., 1994, "Identification of Polysialic Acid-Containing Glycoprotein in the Jelly Coat of Sea-Urchin Eggs—Occurrence of a Novel Type of Polysialic Acid Structure," J. Biol. Chem., **269**(36), pp. 22712–22718.

[2] KitazumeKawaguchi, S., Inoue, S., Inoue, Y., and Lennarz, W. J., 1997, "Identification of Sulfated Oligosialic Acid Units in the O-linked Glycan of the Sea Urchin Egg Receptor for Sperm," Proc. Natl. Acad. Sci. U.S.A., **94**(8), pp. 3650–3655.

[3] Vacquier, V. D., and Moy, G. W., 1997, "The Fucose Sulfate Polymer of Egg Jelly Binds to Sperm Rej and is the Inducer of the Sea Urchin Sperm Acrosome Reaction," Dev. Biol., **192**(1), pp. 125–135.

[4] Bonnell, B. S., Larabell, C., and Chandler, D. E., 1993, "The Sea-Urchin Egg Jelly Coat is a 3-Dimensional Fibrous Network as Seen by Intermediate Voltage Electron-Microscopy and Deep-Etching Analysis," Mol. Reprod. Dev., **35**(2), pp. 181–188.

[5] Bonnell, B. S., Keller, S. H., Vacquier, V. D., and Chandler, D. E., 1994, "The Sea-Urchin Egg Jelly Coat Consists of Globular Glycoproteins Bound to a Fibrous Fucan Superstructure," Dev. Biol., **162**(1), pp. 313–324.

[6] Bonnell, B. S., Reinhart, D., and Chandler, D. E., 1996, "Xenopus Laevis Egg Jelly Coats Consist of Small Diffusible Proteins Bound to a Complex System of Structurally Stable Networks Composed of High-Molecular-Weight Glycoconjugates," Dev. Biol., **174**(1), pp. 32–42.

[7] Ward, G. E., Brokaw, C. J., Garbers, D. L., and Vacquier, V. D., 1985, "Chemotaxis of Arbacia Punctulata Spermatozoa to Resact, a Peptide From the Egg Jelly Layer," J. Cell Biol., **101**(6), pp. 2324–2329.

[8] Shimomura, H., Suzuki, N., and Garbers, D. L., 1986, "Derivatives of Speract Are Associated With the Eggs of Lytechinus Pictus Sea Urchins," Peptides, **7**(3), pp. 491–495.

[9] Cook, S. P., Brokaw, C. J., Muller, C. H., and Babcock, D. F., 1994, "Sperm Chemotaxis—Egg Peptides Control Cytosolic Calcium to Regulate Flagellar Responses," Dev. Biol., **165**(1), pp. 10–19.

[10] Shimomura, H., and Garbers, D. L., 1986, "Differential-Effects of Resact Analogs on Sperm Respiration Rates and Cyclic-Nucleotide Concentrations," Biochemistry, **25**(11), pp. 3405–3410.

[11] Suzuki, N., and Garbers, D. L., 1984, "Stimulation of Sperm Respiration Rates by Speract and Resact at Alkaline Extracellular Ph," Biol. Reprod., **30**(5), pp. 1167–1174.

[12] Suzuki, N., Shimomura, H., Radany, E. W., Ramarao, C. S., Ward, G. E., Bentley, J. K., and Garbers, D. L., 1984, "A Peptide Associated With Eggs Causes a Mobility Shift in a Major Plasma-Membrane Protein of Spermatozoa," J. Biol. Chem., **259**(23), pp. 4874–4879.

[13] Gould, M. C., and Stephano, J. L., 2003, "Polyspermy Prevention in Marine Invertebrates," Microsc. Res. Tech., **61**(4), pp. 379–388.

[14] Podolsky, R. D., 1995, *Consequences of Temperature, Viscosity, and Small Size for Early Life-History Processes in the Sand Dollar Dendraster Excentricus*, University of Washington, Seattle, p. 130.

[15] Styan, C. A., 1998, "Polyspermy, Egg Size, and the Fertilization Kinetics of Free-Spawning Marine Invertebrates," Am. Nat., **152**(2), pp. 290–297.

[16] Levitan, D. R., 2002, "The Relationship Between Conspecific Fertilization Success and Reproductive Isolation Among Three Congeneric Sea Urchins," Evolution (Lawrence, Kans.), **56**(8), pp. 1599–1609.

[17] Podolsky, R. D., and Strathmann, R. R., 1996, "Evolution of Egg Size in Free-Spawners: Consequences of the Fertilization-Fecundity Trade-Off," Am. Nat., **148**(1), pp. 160–173.

[18] Podolsky, R. D., 2001, "Evolution of Egg Target Size: An Analysis of Selection on Correlated Characters," Evolution (Lawrence, Kans.), **55**(12), pp. 2470–2478.

[19] Farley, G. S., and Levitan, D. R., 2001, "The Role of Jelly Coats in Sperm-Egg Encounters, Fertilization Success, and Selection on Egg Size in Broadcast Spawners," Am. Nat., **157**(6), pp. 626–636.

[20] Alves, A. P., Mulloy, B., Diniz, J. A., and Mourao, P. A. S., 1997, "Sulfated Polysaccharides From the Egg Jelly Layer are Species-Specific Inducers of Acrosomal Reaction in Sperms of Sea Urchins," J. Biol. Chem., **272**(11), pp. 6965–6971.

[21] Alves, A. P., Mulloy, B., Moy, G. W., Vacquier, V. D., and Mourao, P. A. S., 1998, "Females of the Sea Urchin Strongylocentrotus Purpuratus Differ in the Structures of Their Egg Jelly Sulfated Fucans," Glycobiology, **8**(9), pp. 939–946.

[22] Kamei, N., and Glabe, C. G., 2003, "The Species-Specific Egg Receptor for Sea Urchin Sperm Adhesion Is Ebr1, a Novel Adamts Protein," Genes Dev., **17**(20), pp. 2502–2507.

[23] Bolton, T., and Thomas, F. I. M., 1999, "Extracellular Structures Surrounding Echinoid Eggs Mitigate the Transmission of Compressive Forces to Eggs," Am. Zool., **39**(5), pp. 132A–132A.

[24] Bolton, T. F., and Thomas, F. I. M., 2002, "Physical Forces Experienced by Echinoid Eggs in the Oviduct During Spawning: Comparison of the Geminate Pair Echinometra Vanbrunti and Echinometra Lucunter," J. Exp. Mar. Biol. Ecol., **267**(2), pp. 123–137.

[25] Thomas, F. I. M., and Bolton, T. F., 2000, "Mechanical Forces Imposed on Echinoid Eggs During Spawning: Mitigation of Force by Fibrous Networks Within Egg Extracellular Layers," Am. Zool., **40**(6), pp. 1232–1233.

[26] Thomas, F. I. M., and Bolton, T. F., 1999, "Shear Stress Experienced by Echinoderm Eggs in the Oviduct During Spawning: Potential Role in the Evolution of Egg Properties," J. Exp. Biol., **202**(22), pp. 3111–3119.

[27] Thomas, F. I. M., Edwards, K. A., Bolton, T. F., Sewell, M. A., and Zande, J. M., 1999, "Mechanical Resistance to Shear Stress: The Role of Echinoderm Egg Extracellular Layers," Biol. Bull., **197**(1), pp. 7–10.

[28] Thomas, F. I. M., Bolton, T. F., and Sastry, A. M., 2001, "Mechanical Forces Imposed on Echinoid Eggs During Spawning: Mitigation of Forces by Fibrous Networks Within Egg Extracellular Layers," J. Exp. Biol., **204**(5), pp. 815–821.

[29] Denny, M., Dairiki, J., and Distefano, S., 1992, "Biological Consequences of Topography on Wave-Swept Rocky Shores.1. Enhancement of External Fertilization," Biol. Bull., **183**(2), pp. 220–232.

[30] Mathur, A. B., Collinsworth, A. M., Reichert, W. M., Kraus, W. E., and Truskey, G. A., 2001, "Endothelial, Cardiac Muscle and Skeletal Muscle Exhibit Different Viscous and Elastic Properties as Determined by Atomic Force Microscopy," J. Biomech., **34**(12), pp. 1545–1553.

[31] Sen, S., Subramanian, S., and Discher, D. E., 2005, "Indentation and Adhesive Probing of a Cell Membrane With AFM: Theoretical Model and Experiments," Biophys. J., **89**(5), pp. 3203–3213.

[32] Bausch, A. R., Ziemann, F., Boulbitch, A. A., Jacobson, K., and Sackmann, E., 1998, "Local Measurements of Viscoelastic Parameters of Adherent Cell Sur-

faces by Magnetic Bead Microrheometry," Biophys. J., **75**(4), pp. 2038–2049.
[33] Chesla, S. E., Selvaraj, P., and Zhu, C., 1998, "Measuring Two-Dimensional Receptor-Ligand Binding Kinetics by Micropipette," Biophys. J., **75**(3), pp. 1553–1572.
[34] Thoumine, O., and Ott, A., 1997, "Time Scale Dependent Viscoelastic and Contractile Regimes in Fibroblasts Probed by Microplate Manipulation," J. Cell. Sci., **110**(17), pp. 2109–2116.
[35] Helfer, E., Harlepp, S., Bourdieu, L., Robert, J., MacKintosh, F. C., and Chatenay, D., 2001, "Viscoelastic Properties of Actin-Coated Membranes," Phys. Rev. E, **63**(1), pp. 021904.
[36] Bao, G., and Suresh, S., 2003, "Cell and Molecular Mechanics of Biological Materials," Nat. Mater., **2**(11), pp. 715–725.
[37] Van Vliet, K. J., Bao, G., and Suresh, S., 2003, "The Biomechanics Toolbox: Experimental Approaches for Living Cells and Biomolecules," Acta Mater., **51**(19), pp. 5881–5905.
[38] Neal, C. R., and Bates, D. O., 2002, "Measurement of Hydraulic Conductivity of Single Perfused Rana Mesenteric Microvessels Between Periods of Controlled Shear Stress," J. Physiol. (London), **543**(3), pp. 947–957.
[39] Wolpert, L., Marsland, D., and Hirshfie, M., 1971, "Effect of High Hydrostatic Pressure on Mechanical Properties of Surface of Sea-Urchin Egg," J. Cell. Sci., **8**(1), pp. 87-92.
[40] Davidson, L. A., Oster, G. F., Keller, R. E., and Koehl, M. A. R., 1999, "Measurements of Mechanical Properties of the Blastula Wall Reveal Which Hypothesized Mechanisms of Primary Invagination Are Physically Plausible in the Sea Urchin Strongylocentrotus Purpuratus," Dev. Biol., **209**(2), pp. 221–238.
[41] Kim, T., Wang, C. W., Lamberson, L., Sastry, A. M., and Thomas, F. I. M., 2005, "The Mechanical Response of the Extracellular Layers of Sea Urchin Eggs Under Shear Flow: A Possible Selective Role in Echinoderm Jelly Coats.," (unpublished).
[42] Caille, N., Thoumine, O., Tardy, Y., and Meister, J. J., 2002, "Contribution of the Nucleus to the Mechanical Properties of Endothelial Cells," J. Biomech., **35**(2), pp. 177–187.
[43] Sastry, A. M., Wang, C. W., and Berhan, L., 2001, "Deformation and Failure in Stochastic Fibrous Networks: Scale, Dimension and Application," *Probabilistic Methods in Fatigue and Fracture. Key Engineering Materials*, Trans Tech, Zurich-Uetikon, pp. 229–250.
[44] Seshaiyer, P., and Humphrey, J. D., 2003, "A Sub-Domain Inverse Finite Element Characterization of Hyperelastic Membranes Including Soft Tissues," ASME J. Biomech. Eng., **125**(3), pp. 363–371.
[45] Kauer, M., Vuskovic, V., Dual, J., Szekely, G., and Bajka, M., 2002, "Inverse Finite Element Characterization of Soft Tissues," J. Interv Card. Electrophysiol., **6**(3), pp. 275–287.
[46] Pruppacher, H. R., Le Clair, B. P., and Hamielec, A. E., 1970, "Some Relations Between Drag and Flow Pattern of Viscous Flow Past a Sphere and a Cylinder at Low and Intermediate Reynolds Numbers," J. Fluid Mech., **44**, pp. 781–790.